Published OnlineFirst June 12, 2020; DOI: 10.1158/0008-5472.CAN-19-3599

Engineering the Human Fc Region Enables Direct Cell Killing by Cancer Glycan–Targeting Antibodies without the Need for Immune Effector Cells or Complement

Mireille Vankemmelbeke[1,2], Richard S. McIntosh[1], Jia Xin Chua[1,2], Thomas Kirk[1,2], Ian Daniels[2], Marilena Patsalidou[1], Robert Moss[1], Tina Parsons[2], David Scott[3], Gemma Harris[4], Judith M. Ramage[1], Ian Spendlove[1], and Lindy G. Durrant[1,2]

ABSTRACT

Murine IgG3 glycan-targeting mAb often induces direct cell killing in the absence of immune effector cells or complement via a proinflammatory mechanism resembling oncotic necrosis. This cancer cell killing is due to noncovalent association between Fc regions of neighboring antibodies, resulting in enhanced avidity. Human isotypes do not contain the residues underlying this cooperative binding mode; consequently, the direct cell killing of mouse IgG3 mAb is lost upon chimerization or humanization. Using the Lewis$^{a/c/x}$ -targeting 88mAb, we identified the murine IgG3 residues underlying the direct cell killing and increased avidity via a series of constant region shuffling and subdomain swapping approaches to create improved ("i") chimeric mAb with enhanced tumor killing *in vitro* and *in vivo*. Constant region shuffling identified a major CH3 and a minor CH2 contribution, which was further mapped to discontinuous regions among residues 286–306 and 339–378 that, when introduced in 88hIgG1, recapitulated the direct cell killing and avidity of 88mIgG3. Of greater interest was the creation of a sialyl-di-Lewis^{a}–targeting i129G1 mAb via introduction of these selected residues into 129hIgG1, converting it into a direct cell killing mAb with enhanced avidity and significant *in vivo* tumor control. The human iG1 mAb, termed Avidimabs, retained effector functions, paving the way for the proinflammatory direct cell killing to promote antibody-dependent cellular cytotoxicity and complement-dependent cytotoxicity through relief of immunosuppression. Ultimately, Fc engineering of human glycan-targeting IgG1 mAb confers proinflammatory direct cell killing and enhanced avidity, an approach that could be used to improve the avidity of other mAb with therapeutic potential.

Significance: Fc engineering enhances avidity and direct cell killing of cancer-targeting anti-glycan antibodies to create superior clinical candidates for cancer immunotherapy.

Introduction

The cancer glycome is a rich source of targets for mAb development due to the alterations associated with the transformation process, as well as glycans being key coaccessory molecules for cancer cell survival, proliferation, dissemination, and immune evasion (1, 2). A number of anti-glycan mAbs are in clinical development, as passive or active immunotherapy or reformatted for chimeric antigen receptor T cells (3–5). In addition, Dinutuximab beta, an anti-GD2 mAb, is currently used for the treatment of neuroblastoma (6).

We previously described a panel of cancer glycan–targeting mAbs with Lewis$^{a/c/x}$, Lewis^{y} (7, 8) as well as sialyl-di-Lewis^{a} reactivity (9). Intriguingly, some of these glycan-binding mAbs exhibited a direct cytotoxic effect on high-density target-expressing cancer cells, independent of the presence of complement or immune effector cells. This direct cytotoxic ability has also been observed for other anti-glycan mAbs and typically involves mAb-induced homotypic cellular adhesion, cytoskeletal rearrangement followed by cell swelling, membrane lesions, and eventual cellular demise (7, 10–13). In most cases, the cell death is a form of nonclassical apoptosis, potentially involving the generation of reactive oxygen species and most closely resembling oncotic necrosis (14, 15). Importantly, akin to immunogenic or inflammatory cell death, the coinciding release of in inflammatory mediators—damage-associated molecular patterns (DAMP)—has the potential to recruit innate immune cells to the tumor site that may further increase mAb-mediated effector functions (16). Thus, these anti-glycan mAbs can be important tools to remobilize the full potential of the immune system in an otherwise immunosuppressive environment.

The direct killing ability of anti-glycan mAbs is mediated by murine (m) IgG3, an isotype that exhibits noncovalent interactions between adjacent Fc regions, thereby increasing avidity, via prolonging target occupancy, a process termed "intermolecular co-operativity" (17, 18). In humans, the IgG2 isotype can increase avidity via dimerization involving one or more Cys residues in its hinge region (19). However, this inefficient process, combined with poor antibody-dependent cellular cytotoxicity (ADCC) and complement-dependent cytotoxicity (CDC) activity, renders the hIgG2 an unattractive clinical candidate.

Our panels of mAbs induce strong *in vitro* and *in vivo* tumor killing in preclinical mouse models (7, 8) and thus are candidates for clinical development. Chimerization of the mIgG3 mAbs onto a human IgG1 backbone coincided with a dramatic reduction in direct cytotoxicity,

[1]Academic Department of Clinical Oncology, Division of Cancer and Stem Cells, School of Medicine, University of Nottingham Biodiscovery Institute, University Park, Nottingham, United Kingdom. [2]Scancell Limited, University of Nottingham Biodiscovery Institute, University Park, Nottingham, United Kingdom. [3]School of Biosciences, University of Nottingham, Sutton Bonington Campus, United Kingdom. [4]Research Complex at Harwell, Rutherford Appleton Laboratory, Didcot, United Kingdom.

Note: Supplementary data for this article are available at Cancer Research Online (http://cancerres.aacrjournals.org/).

M. Vankemmelbeke and R.S. McIntosh contributed equally to this article.

Corresponding Author: Lindy G. Durrant, University of Nottingham, University Park, Nottingham NG7 2RD, United Kingdom. Phone: 44-0-115-8231863; E-mail: lindy.durrant@nottingham.ac.uk

Cancer Res 2020;80:3399–412

doi: 10.1158/0008-5472.CAN-19-3599

Published OnlineFirst June 12, 2020; DOI: 10.1158/0008-5472.CAN-19-3599

leading us to hypothesize that this was the result of diminished intermolecular cooperativity. Consequently, the rationale for this study was to identify the key residues within mIgG3 that are responsible for noncovalent Fc interactions and transfer them into hIgG1 in order to recapitulate the mIgG3-observed direct cytotoxicity and avidity, thereby creating a chimeric hIgG1 with superior clinical utility.

We report here the identification of discontinuous regions within the mIgG3 CH2 and CH3 domains that endow this isotype with direct cytotoxicity and increased avidity. Transfer of these residues into the hIgG1 isotype creates an improved "i"hIgG1 with increased *in vitro* and *in vivo* antitumor activity.

Materials and Methods

Materials, cells, and antibodies

Colorectal cancer cell lines (COLO205 and HCT15) as well as the murine myeloma NS0 cell line were purchased from the ATCC. All cell lines were authenticated using short tandem repeat profiling and tested monthly for the presence of Mycoplasma. Human serum albumin (HSA)-APD-sialyl-Lewis^a and HSA-APD-Lewis^a were from IsoSepAB. Cell lines were maintained in RPMI medium 1640 (Sigma) supplemented with 10% FCS, L-glutamine (2 mmol/L), and sodium bicarbonate-buffered. Parental murine FG88.2 and FG129 mAbs were generated, as previously described (7, 9).

Cloning of modified mAb constructs

In order to create chimeric hIgG1 variants of our hybridoma-produced mAbs (FG88.2 and FG129), the heavy-chain and light-chain variable regions encoding the respective mAbs were introduced into the pDCOrig vector using the restriction enzymes BamHI/BsiWI (light-chain locus) or HindIII/AfeI (heavy-chain locus; ref. 20). The synthetic heavy-chain constant regions (CH), including full mIgG3 constant regions as well as interchanged mIgG3-hIgG1 domains and single residue changes, were designed and ordered from Eurofins MWG. Typically, this involved a 1,054 bp cassette supplied in proprietary Eurofins vectors, stretching from the AfeI restriction site at the VH/CH junction to an XbaI site 3′ to the CH stop codon. After maxiprep (Qiagen), 15 μg of plasmid DNA was digested with AfeI and XbaI (NEB) and the insert gel–purified (QIAquick, Qiagen) and introduced into AfeI/XbaI-digested vector pOrigHiB (20) by ligation (T4 DNA ligase, NEB). Following sequence confirmation, 15 μg of plasmid DNA was digested with AfeI and AvrII (NEB) and the insert introduced into AfeI/AvrII-digested vector pDCOrig by ligation. A cartoon representation of the key Fc-engineered constructs is shown in Supplementary Fig. S1.

HEK293 transfection and mAb purification

MAb constructs were obtained following transient transfections of Expi293F cells using the ExpiFectamine 293 Transfection kit (Gibco, Life Technologies). Briefly, HEK293 cells in suspension (100 mL, 2×10^6/mL) were transfected with 100 μg DNA and conditioned medium harvested at day 7 after transfection. mAb-containing supernatant was filtered through 0.22 μm bottle top filters (Merck Millipore), and sodium azide was added to a final concentration of 0.2% (w/v). mAb was purified on protein G columns (HiTrap ProteinG HP, GE Healthcare) using an AKTA FPLC (GE Healthcare). Columns were washed with PBS/Tris buffer (PBS with 50 mmol/L Tris/HCl, pH 7.0) before mAb elution with a rapid gradient into 100 mmol/L glycine, pH 12 (supplemented with 0.05% v/v Tween 20), collecting 2 mL fractions. Fractions containing mAb were pooled, neutralized to pH 7.0 (using 1 mol/L HCl), and dialyzed against PBS, before concentration determination and storage at −80°C. All transiently expressed mAb constructs were analyzed for cell binding using flow cytometry, as a readout for correct folding, and compared with the parental 88mIgG3 and 88hIgG1, prior to use in functional assays.

Indirect immunofluorescence and flow cytometry

Cancer cells (1×10^5) were incubated with primary mAbs (at 33.3 nmol/L or titrated) for 1 hour at 4°C, as previously described (7) followed by 1-hour incubation at 4°C with anti-mouse or anti-human FITC-labeled secondary antibody and fixing in 0.4% formaldehyde. Stained samples were analyzed on a MACSQuant 10 flow cytometer and analyzed using FlowJo v10.

Avidity determination

The kinetic parameters of the 88 and 129 mAbs binding to Lewis^a- or sialyl-Lewis^a-APD-HSA were determined by Surface Plasmon Resonance (SPR, Biacore 3000, GE Healthcare). Increasing concentrations (0.3–200 nmol/L) of mAb were injected across a CM5 chip, and data were fitted to a heterogeneous ligand binding model using BIAevaluation 4.1. The chip contained four cells, two of which were HSA-coated (in-line reference cells), and the other two were coated with low [30–80 response units (RU)] and high amounts (360–390 RU) of the respective glycan-APD-HSA.

In vitro cytotoxicity

Propidium iodide (PI) uptake and proliferation inhibition were performed to analyze the direct cytotoxic effect of the mAbs. COLO205 or HCT15 cells (5×10^4) were incubated with mAbs for 2 hours at 37°C followed by the addition of 1 μg of PI for 30 minutes. Cells were resuspended in PBS and run on a Beckman Coulter FC-500 or on a MACSQuant 10 flow cytometer and analyzed with WinMDI 2.9 or FlowJo v10 software, respectively. Proliferation inhibition was assessed by using the water-soluble tetrazolium salt WST-8 (CCK8 kit; Sigma-Aldrich) to measure the activity of cellular hydrogenases, which is directly proportional to the number of viable cells. Briefly, after overnight plating of cancer cells (1,000 cells/90 μL/well), constructs were added at different concentrations in a final volume of 10 μL/well and the plates were incubated at 37°C (5% CO_2) for 72 to 96 hours. WST-8 reagent was then added (10 μL/well), and after a further 3-hour incubation, the plates were read at 450 nm (Tecan Infinite F50) and percentage inhibition calculated. EC_{50} values were determined using nonlinear regression (curve fit) with GraphPad Prism v 8.0 (GraphPad Inc.).

Immune effector function determination

ADCC and CDC were performed as described previously (7). ^{51}Cr-labeled target cells (5×10^3) were coincubated with 100 μL of peripheral blood mononuclear cells from healthy donors (ADCC) or 10% (v/v) autologous serum (CDC) and with mAbs at a range of concentrations; the effector to target ratio was 100:1 (E:T). Spontaneous and maximum release [counts per minute (cpm)] was evaluated by incubating the labeled cells with medium or with 10% (v/v) Triton X-100, respectively. The mean percentage lysis was calculated as follows: mean % lysis = (experimental cpm - spontaneous cpm)/(maximum cpm − spontaneous cpm) × 100.

Scanning electron microscopy

HCT15 or COLO205 cells (1×10^5) were grown on sterile coverslips for 24 hours prior to mAb (0.2 μmol/L) addition for 18 hours at 37°C. Controls included medium alone and 0.5% (v/v) hydrogen peroxide (H_2O_2; Sigma). Cells were washed with prewarmed 0.1 mol/L sodium cacodylate buffer pH 7.4 (SDB) and fixed with 12.5% (v/v)

glutaraldehyde for 24 hours. Fixed cells were washed twice with SDB and postfixed with 1% (v/v) osmium tetroxide (pH 7.4) for 45 minutes. After a final wash with H_2O, the cells were dehydrated in increasing concentrations of ethanol and exposed to critical point drying, before sputtering with gold, prior to SEM analysis (JSM-840 SEM, JEOL).

Recombinant human FcRn binding analysis

The ability of the mAbs to bind to recombinant human (rh) FcRn (R&D Systems) was evaluated using direct ELISA at pH 6.0 and pH 7.0. Briefly, high-binding ELISA plates were coated with 250 ng/well rhFcRn followed by blocking with protein-free blocking buffer (Thermo Fisher Scientific). Primary mAb dilutions (in phosphate buffer pH 6.0 or pH 7.0) were added (1 hour at room temperature), followed by washing with respective phosphate buffers containing 0.05% (v/v) Tween 20, and detection of bound mAbs with goat $F(ab)_2$ anti-human $IgG(Fab)_2$ HRP antibody (Abcam). The anti-hCTLA4 hIgG1 mAb ipilimumab (clinical grade) was included as a positive control.

Biophysical characterization of the mAbs (size exclusion chromatography with multiangle light scattering and analytical ultracentrifugation)

Size exclusion chromatography with multiangle light scattering (SEC-MALS) experiments were performed using a Superose 6 10/300 Increase column (GE Healthcare) on an AktaPure 25 System (GE Healthcare). mAb samples (100 µL at 1 mg/mL) were loaded and eluted with one column volume (24 mL) of buffer, at a flow rate of 0.5 mL/min. The eluting protein was monitored using a DAWN HELEOS-II 18-angle light scattering detector (Wyatt Technologies) equipped with a WyattQELS dynamic light scattering module, a U9-M UV/Vis detector (GE Healthcare), and an Optilab T-rEX refractive index monitor (Wyatt Technologies). Data were analyzed by using Astra (Wyatt Technologies) using a refractive index increment value of 0.185 mL/g.

For analytical ultracentrifugation (AUC) characterization, sedimentation velocity scans were recorded for each mAb sample at concentrations of 5.0, 2.5, and 0.5 µmol/L. All experiments were performed at 50,000 rpm, using a Beckman Optima analytical ultracentrifuge with an An-50Ti rotor at 20°C. Data were recorded using the absorbance optical detection system at 280 nm. The density and viscosity of the buffer were measured experimentally using a DMA 5000M densitometer equipped with a Lovis 200ME viscometer module. The partial specific volume of the antibodies was calculated using SEDFIT from the amino acid sequence. Data were processed using SEDFIT, fitting to the c(s) model. Figures were made using GUSSI.

C4d ELISA

Complement activation in normal human serum, in the absence of target, was determined by measuring C4d concentrations, a marker for classical complement pathway activation. mAbs (10% v/v, 100 µg/mL) were incubated in 90% normal human serum (three healthy donors) for 1 hour at 37°C. C4d concentrations were measured using a commercial ELISA kit (MicroVue C4d EIA kit, Quidel Corporation) according to the manufacturer's instructions. Heat-aggregated (HA) mAb served as a positive control; the anti-hCTLA4 hIgG1 mAb ipilimumab (clinical grade) as a reference.

In vivo model

The study was conducted and approved by CrownBio UK under a UK Home Office Licence in accordance with National Cancer Research Institute, Laboratory Animal Science Association, and Federation for Laboratory Animal Science Associations guidelines. Animal welfare for this study complies with the UK Animals Scientific Procedures Act 1986 (ASPA) in line with Directive 2010/63/EU of the European Parliament and the Council of September 22, 2010, on the protection of animals used for scientific purposes. Subcutaneous tumors of a human colorectal adenocarcinoma model of COLO205 were established in age-matched female BALB/c nude (Charles River) mice via injection of 5×10^6 viable cells in 0.1 mL serum-free RPMI: Matrigel (1:1) into the left flank of each mouse. Mice ($n = 10$) were randomly allocated to treatment groups based on their mean tumor volume ($\sim$103 $mm^3 \pm 13$ mm^3) on study day 6 and dosed i.v., biweekly, with mAbs (0.1 mg) or vehicle (PBS, 100 µL) up until week 5. Body weight and tumor volume were assessed 3 times weekly, and reduction in tumor volume was analyzed statistically using two-way ANOVA with Bonferroni's post-test at day 35, when all control animals were still in the study (GraphPad Prism v 7.4, GraphPad Inc.).

Statistical analyses

The error bars shown in the figures represent the mean $\pm$ SD. Titration curves for functional assays (direct cell killing, immune effector functions) were analyzed with two-way ANOVA with the construct factor *P* values graphed. Functional affinity results as well as fixed-concentration functional assays were analyzed with one-way ANOVA with Dunnett's corrections for multiple comparisons. All analyses were performed with GraphPad Prism v 7.4 (GraphPad Inc.), with *, $P \le 0.05$; **, $P \le 0.01$; ***, $P \le 0.001$; and ****, $P \le 0.0001$.

Results

m88G3 exhibits avid glycan binding as well as direct cytotoxicity in the absence of complement and immune effector cells, both of which are reduced upon chimerization to 88hIgG1

We have previously shown that the hybridoma-produced mIgG3 mAb FG88.2 exerts a direct cytotoxic effect on high-binding cancer cell lines, such as COLO205 and HCT15, in the absence of complement or effector cells (7). This direct cytotoxicity involved mAb-induced cellular aggregation, proliferation inhibition as well as irregular pore formation through an oncolytic mechanism. We subsequently created a chimeric, HEK293-expresssed, hIgG1 mAb, 88hIgG1, for clinical exploitation. 88hIgG1 maintained equivalent HCT15 and COLO205 cancer cell binding levels (**Fig. 1A**), compared with the hybridoma-produced FG88.2, as well as the HEK293-expressed 88mIgG3. The latter mAb was generated to rule out expression system-related effects such as differential Fc glycosylation, due to the use of murine hybridoma cells versus HEK293 cells. Surprisingly, 88hIgG1 exhibited significantly reduced direct cytotoxicity on COLO205 and HCT15, across two functional assays, PI uptake and proliferation inhibition, compared with 88mIgG3 (**Fig. 1B–D**). 88mIgG3 also displayed a modest reduction in direct cytotoxicity compared with the hybridoma-produced FG88.2, suggesting that differential glycosylation of the Fc region by the two expression settings (mouse hybridoma vs. HEK293 cells) contributed to the effect. Combined, the results indicated that the direct cell killing could be related to the kinetic binding behavior of the different isotypes. Consequently, the kinetic binding of our isotype-switched mAbs was analyzed on a Lewis^a-APD-HAS–coated chip using SPR (Supplementary Table S1). FG88.2 displayed avid Lewis^a-APD-HSA binding with fast apparent on-rates ($k_{on} \sim 10^4$ 1/smol/L) and very slow off-rates ($k_{off} \sim 10^{-6}$ 1/s) on the high-density flow cell. The HEK293-produced 88mIgG3 exhibited an apparent faster on-rate ($k_{on} \sim \times 10^5$ 1/smol/L) and a somewhat faster off-rate ($k_{off} \sim 10^{-4}$ 1/s) compared with FG88.2, which could explain the slightly reduced cytotoxicity compared with FG88.2. In comparison, 88hIgG1 bound its target with an apparent fast on-rate ($k_{on} \sim 10^5$ 1/smol/L), but in

Published OnlineFirst June 12, 2020; DOI: 10.1158/0008-5472.CAN-19-3599

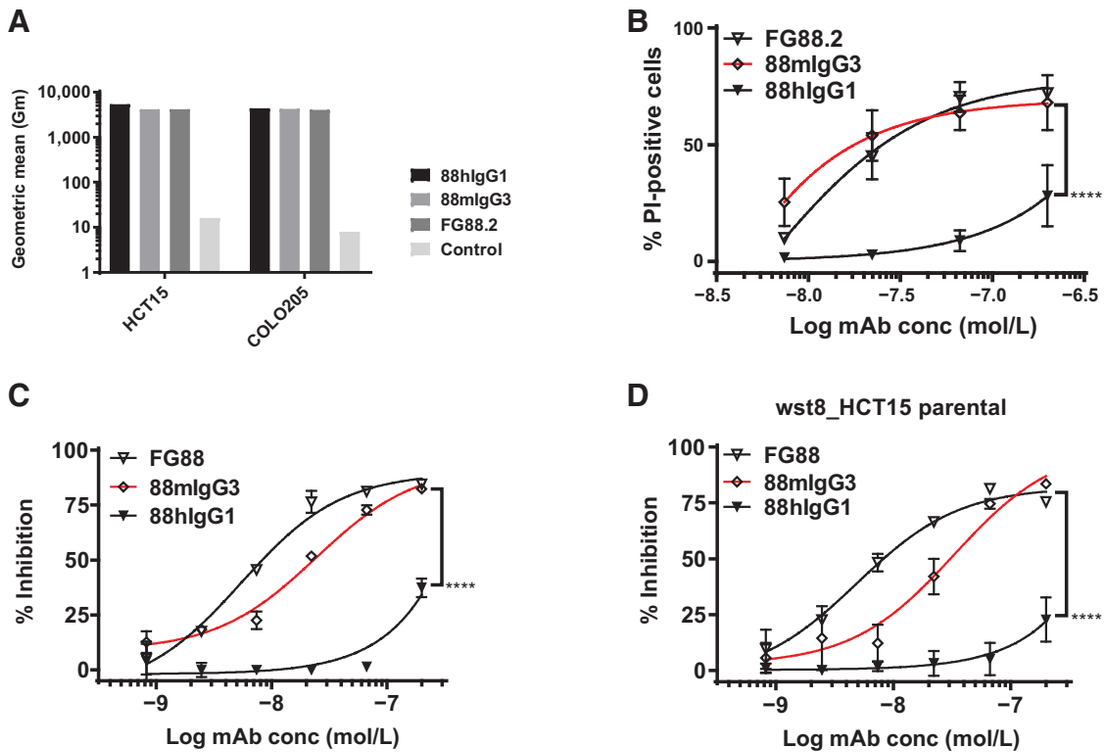

Figure 1.

Maintenance of cancer cell binding, but significantly decreased direct cytotoxicity of 88hIgG1 compared with 88mIgG3 and parental hybridoma mAb, FG88.2. **A,** Comparable HCT15 and COLO205 cell binding by 88hIgG1, 88mIgG3, and FG88.2 (hybridoma mAb). **B,** Significantly reduced direct cytotoxicity (PI uptake) on HCT15 by 88hIgG1 compared with 88mIgG3 and FG88.2. **C** and **D,** Significantly reduced proliferation inhibition by 88hIgG1 compared with 88mIgG3 and FG88.2 on COLO205 (**C**) and HCT15 (**D**). Significance (88hIgG1 compared with 88mIgG3) deduced from two-way ANOVA. ****, $P \leq 0.0001$.

contrast to the mIgG3 isotypes displayed a much faster dissociation phase (apparent $k_{off} \sim 10^{-2}$ 1/s), that is likely to underlie its reduced cytotoxic activity upon cancer cell binding. The mAb binding behavior on the low-density flow cell was largely comparable between the three mAbs, with equilibrium dissociation constants (Kd) of the order of 10^{-8} mol/L for all three isotypes.

Domain analysis of the mIgG3 constant region indicates a major contribution by the mIgG3 CH3 domain with a minor involvement of the CH2

Collectively, the results outlined above suggested that the high Lewis^a-APD-HSA avidity exhibited by FG88.2 and 88mIgG3, predominantly driven by their slow target dissociation and potentially resulting from the intermolecular cooperativity of the mIgG3 isotype, contributed to their direct cytotoxic effect. We thus set out to engineer a hIgG1 cancer glycan–targeting mAb with direct cytotoxic activity, via the transfer of selected mIgG3 constant region residues into 88hIgG1. Firstly, mIgG3 contributing regions were identified through the creation of hybrid 88hIgG1 constructs, containing mIgG3 CH1, CH2, or CH3 domains. Preliminary analyses ascertained that mIgG3 CH1 had a negligible contribution to the direct cytotoxicity ability of 88mIgG3, as introducing mIgG3 CH1 into 88hIgG1 (1m1) did not lead to a significant increase in cytotoxicity (**Fig. 2A** and **B**). Conversely, introducing hIgG1 CH1 into 88mIgG3 (3h1), equally, did not instigate a significant reduction in killing activity (**Fig. 2A** and **B**). Next, in a gain-of-function approach, the mIgG3 CH2 and CH3 domains, separately, were introduced in 88hIgG1. 88hIgG1 containing murine CH3 (1m3) exhibited a significant gain in PI uptake on HCT15, as well a significant increased proliferation inhibition of COLO205 cells, when compared with 88hIgG1 (**Fig. 2C** and **D**). Introducing murine CH2 into 88hIgG1 (1m2) led to small, but not significant, increase in killing activity across both assays (**Fig. 2C** and **D**). As a confirmation of the contributions made by both domains, the reverse strategy was adopted, whereby a loss of cytotoxicity activity was evaluated due to the introduction hIgG1 CH2 or CH3 domains into 88mIgG3. This scenario led to a significant decrease in cytotoxicity for 88mG3 containing hIgG1 CH3 (3h3), corroborating the previous gain-of-function results. Importantly, this strategy also identified a small contribution by the murine CH2, as 88mIgG3 containing human CH2 (3h2) exhibited a significant decrease in cytotoxicity activity (**Fig. 2C** and **D**). Next, the kinetic binding behavior of the hybrid constructs was analyzed. The hybrid construct 1m3 exhibited a modest, but significant, increase in avidity (decreased Kd), while 3h3, containing human CH3, displayed a significant decrease in avidity (increased Kd, **Fig. 2E**), in both cases, mirroring the direct cytotoxicity. Human CH2 in construct 3h2 also led to a modest, but significant, drop in avidity. In all cases, the changes in avidity were predominantly driven by changes in the off-rate of the mAbs, with 1m3 showing a significantly decreased off-rate compared with 88hIgG1, whereas 3h3, as well as 3h2, exhibited a significantly increased off-rate compared with 88mIgG3 (**Fig. 2F**). Murine CH2 in construct 1m2 did not lead to increased avidity nor a decreased off-rate, underlying the insignificant cytotoxicity of this construct compared with 88hIgG1 (**Fig. 2C** and **D**). Taken together, the results indicate that the murine CH3 has a more

Published OnlineFirst June 12, 2020; DOI: 10.1158/0008-5472.CAN-19-3599

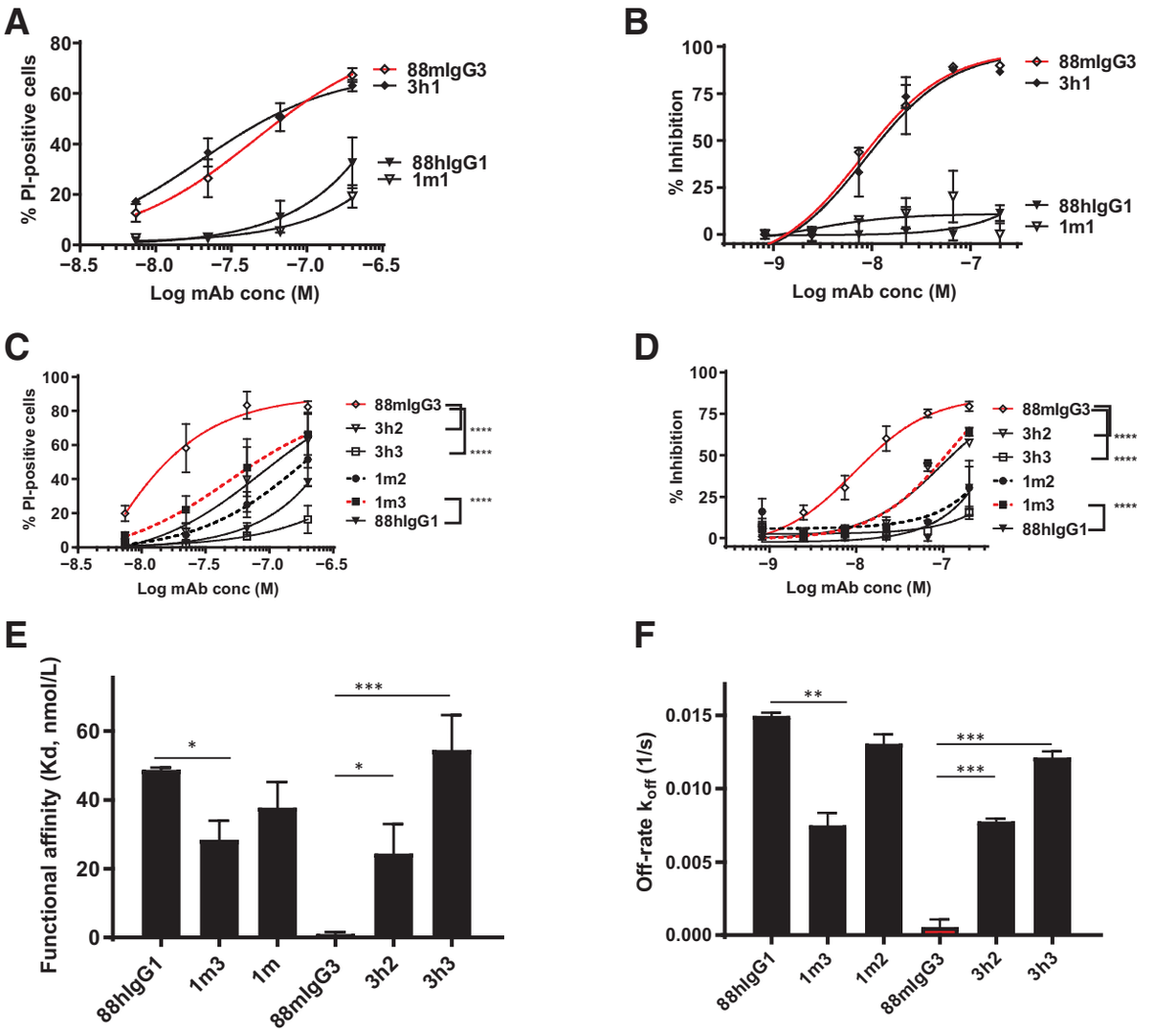

Figure 2.

mIgG3 CH3 and to a lesser extent CH2 contribute to the direct cytotoxicity and improved avidity. **A** and **B,** Constant domain shuffling suggests no significant contribution by CH1 to direct cytotoxicity (PI uptake, HCT15, **A**; proliferation inhibition on COLO205, **B**). **C** and **D,** In contrast, CH3 (1m3 and 3h3) contributes significantly to direct cytotoxicity, with a minor contribution by mCH2 only evident in a loss-of-function approach (3h2; PI uptake, HCT15, **C**; proliferation inhibition, COLO205, **D**). Significance versus the respective parental constructs was deduced from two-way ANOVA. **E** and **F,** Significantly increased avidity and decreased off-rate by 1m3, with significantly decreased avidity and increased off-rate by 3h2 and more pronounced by 3h3, confirming the major CH3 and minor CH2 contributions. Significance deduced using one-way ANOVA, with Dunnett's corrections for multiple comparisons. *, $P \leq 0.05$; **, $P \leq 0.01$; ***, $P \leq 0.001$; ****, $P \leq 0.0001$.

pronounced contribution to cytotoxicity, as well as kinetic binding, whereas the contribution by murine CH2 is smaller, only observed in a loss-of-function setting.

Discontinuous sequences within the CH2-CH3 region of aa 286–397 are essential for killing activity and increased avidity

As the cytotoxic effect endowed by the murine CH3 was not complete, and in order to further narrow down the other contributing residues, we designed hybrid 88 mAb constructs where the CH2 and CH3 domains were further subdivided into two subdomains (SD) with junction regions containing a 10-residue overlap: CH2: SD232-294 and SD286-345 and CH3: SD339-397 and SD390-447. On COLO205, both SD339-397 and SD286-345 afforded a similar significant increase in cytotoxicity, most evident at the lower concentrations, whereas SD232-294, as well as SD390-447, were dispensable for cytotoxicity (**Fig. 3A** and **C**). On HCT15 however, the significant contribution by residues within SD339-397 was larger than that of SD286-345 (**Fig. 3B** and **D**), suggesting that subtle differences in glyco-antigen density and composition can modulate mAb binding and ensuing cytotoxic activity. Strikingly, 88hIgG1, containing the combined mIgG3 SD286-345 and SD339-397 (SD286-397), recovered virtually all the cytotoxicity of 88mIgG3 on both cell lines and across both assays (**Fig. 3A–D**), obviating the need for adding additional subdomains. Avidity analysis of the subdomain constructs, compared with 88hIgG1, revealed a striking improvement in avidity for SD286-397, as well as SD339-397, both now matching the 88mIgG3 avidity, with a more modest

Published OnlineFirst June 12, 2020; DOI: 10.1158/0008-5472.CAN-19-3599

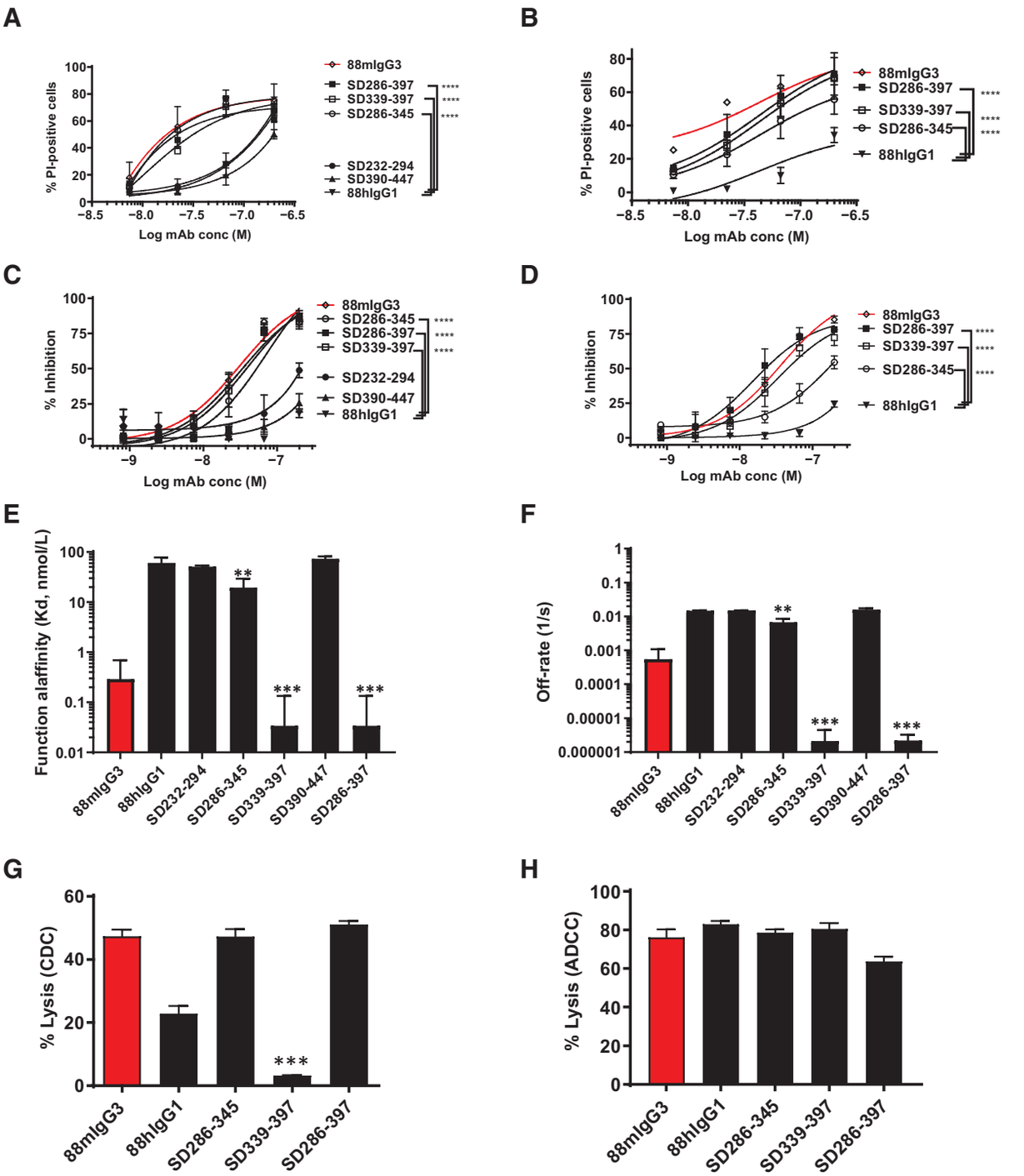

Figure 3.

SD286-397 encompassing the CH2:CH3 junction underlies mIgG3 direct cytotoxicity and improved avidity. Subdomain divisions of CH2CH3 identified two regions that did not contribute, SD232-294 and SD390-447, as well as two regions that significantly contributed to direct cytotoxicity and avidity, SD286-345 (CH2), as well as SD339-397 (CH3). **A** and **B,** Significantly increased PI uptake by both constructs and the combination (SD286-397) compared with 88hIgG1 on COLO205 (**A**) and HCT15 (**B**). **C** and **D,** Significantly increased proliferation inhibition by both constructs and the combination compared with 88hIgG1 on COLO205 (**C**) and HCT15 (**D**). Significance (**A–D**) was deduced from two-way ANOVA. Significantly increased avidity (SPR), resulting mainly from reduced off-rates by SD286-345 and SD339-397, as well as the combination (SD286-397; **E** and **F**, respectively). **G,** Significantly reduced CDC activity (HCT15) by SD339-397 compared with 88hIgG1. **H,** Maintenance of ADCC activity (COLO205) by the aforementioned constructs. Significance versus respective parental constructs (**E–H**) were deduced from one-way ANOVA, with Dunnett's corrections for multiple comparisons. **, $P \leq 0.01$; ***, $P \leq 0.001$; ****, $P \leq 0.0001$.

Published OnlineFirst June 12, 2020; DOI: 10.1158/0008-5472.CAN-19-3599

improvement for SD286-345 (**Fig. 3E**). The improved avidity resulted mainly from a dramatically reduced apparent off-rate ($\sim 10^{-6}$ 1/s) for SD286-397 as well as SD339-397, with the SD286-345 off-rate showing a more modest improvement ($\sim 10^{-3}$ 1/s; **Fig. 3F**). These results add further weight to the cytotoxicity observations and support the notion that creating an mAb with a reduced target dissociation rate upholds direct cytotoxicity.

Although SD339-397, with 27 mIgG3 residues, recapitulated up to 90% of the desirable attributes of 88mIgG3, notably the slow dissociation and enhanced cytotoxicity, it exhibited a significantly reduced CDC activity compared with 88hIgG1 (**Fig. 3G**), but it maintained ADCC activity compared with 88hIgG1 (**Fig. 3H**). The effect on the immune effector functions thus necessitated the use of SD286-397, containing 41 mIgG3 residues for further development. Consequently, additional subdivisions of SD286-345 and SD339-397 were analyzed for cytotoxic activity and avidity in order to further reduce the number of mIgG3 residues. Firstly, within SD339-397, SD339-378, containing 20 mIgG3-specific residues, upon introduction in 88hIgG1 led to a significant regain of cytotoxicity to within approximately 80% to 90% of mIgG3 cytotoxicity across both cytotoxicity assays (**Fig. 4A** and **B**). This region also instilled a significant increase in avidity, compared with 88hIgG1 (**Fig. 4G**), but this improvement was not as pronounced as in the case of SD339-397 (**Fig. 3G**). Immune effector functions (ADCC and CDC) of SD339-378 were not significantly different from 88hIgG1 (**Fig. 4H** and **I**). In addition, within SD286-345, the significant reduction in cytotoxicity by SD307-345, compared with SD286-345, implied a further contribution by residues 286–306 (**Fig. 4C**). Collectively, the results suggested that a construct containing the combination of residues 286–306 and 339–378, totaling 26 mIgG3-specific residues, could potentially fully recapitulate 88mIgG3 direct cytotoxicity and avidity. To test this hypothesis, the cytotoxic activity and avidity of SD286-306+339-378 was evaluated. SD286-306+339-378 exhibited significantly improved direct cytotoxicity, compared with 88 hIgG1, on both cell lines, now matching 88mIgG3 cytotoxicity (**Fig. 4D–F**). SPR analysis of SD286-306+339-378 revealed a significantly improved avidity compared with 88hIgG1 with a Kd (0.3×10^{-9} nmol/L) now similar to 88mIgG3 (**Fig. 4G**). Importantly, neither the CDC activity nor the ADCC activity of the SD286-306+339-378 construct was significantly different from that of 88hIgG1 (**Fig. 4H** and **I**). The combination of improved avidity with direct cytotoxicity, as well as maintained immune effector functions indicates that our SD286-306+339-378 hybrid hIgG1 mimics the desirable attributes of 88mIgG3.

Reversal of one *in silico*–identified MHCII binding cluster generates the lead candidate, improved "i" 88G1, with robust cell killing, increased avidity, pore-forming ability, and sound immune effector functions

We performed an *in silico* screen of the SD286-306+339-378 sequence, containing 26 mIgG3 residues, for MHCII binding epitopes (Immune Epitope Database, IEDB), in order to assess potential immunogenicity. Class II–restricted T helper cells are relevant to the humoral immune response, and predicted binding clusters have been shown to be strong indicators of T-cell responses (21). Two potential MHCII binding clusters were identified: cluster 1 (residues 294–315), which would be potentially immunogenic in a wide range of HLA types, and cluster 2 (residues 365–393), which would potentially only be weakly immunogenic in HLA-DR*0401 and HLA-DR*01101 (Supplementary Fig. S2). Reversion of three murine residues, 294 (A to E), 300 (F to Y), and 305 (A to V), within cluster 1, to human residues, produced a human sequence section to which individuals would have been tolerized. Similarly, reversal to human sequence of two residues 351 (I to L) and 371 (N to G), within cluster 2, removed two potential MHCII binding epitopes. Consequently, we created two additional SD286-306+339-378–based constructs: DI1 and DI2, containing three and two human reverted residues, respectively, and assayed their cytotoxicity and avidity. DI1 maintained significantly improved cytotoxicity compared with 88hIgG1. In addition, the direct cytotoxicity coincided with a favorable avidity profile, with an apparent off-rate of approximately 10^{-4} 1/s and a Kd of 0.5 nmol/L that was similar to 88mIgG3 (**Fig. 5C**; **Table 1**; Supplementary Fig. S3). In contrast, DI2 showed a small, but consistently, decreased activity compared with 88mIgG3 (**Fig. 5A** and **B**) as well as a significantly decreased avidity compared with 88mIgG3 (**Fig. 5C**). As this cluster was only potentially weakly immunogenic in two HLA-DR types, these two residues have not been reverted. Instead, we focused on 88DI1, containing 23 mIgG3 residues, now renamed "i" (improved) 88G1, for further analysis of its immune effector functions. 88hIgG1 showed potent ADCC activity on COLO205 with subnanomolar EC_{50} (**Fig. 5D**), in line with the potent immune effector functions of FG88.2 (7). Similarly, i88G1 displayed potent ADCC with subnanomolar EC_{50} (0.35 nmol/L) albeit significantly reduced compared with 88hIgG1 (EC_{50} 0.13 nmol/L). The CDC activity of i88G1 (EC_{50} 0.1 nmol/L) was significantly improved compared with 88hIgG1 (3.9 nmol/L; **Fig. 5E**; **Table 1**).

Earlier work on the parental hybridoma–produced FG88.2 had demonstrated its pore-forming ability, which was surmised to underlie its cytotoxicity (7). We thus set out to analyze the pore-forming ability of i88G1 on HCT15, using SEM. Incubation of HCT15 with i88G1 or 88mIgG3, but not 88hIgG1, resulted in monolayer disruption, cell rounding, and clustering. At higher magnification, irregular pore formation was evident (**Fig. 5F**), mirroring the original data observed for the hybridoma-produced FG88.2 (7).

Collectively, the results indicate that transfer of selected regions from the mIgG3 constant region into the 88higG1 backbone created a hybrid mAb with direct cell killing ability, increased avidity, pore-forming ability as well as robust immune effector functions.

Transfer of the "iG1" sequences into an alternative, nonkilling, glycan binding mAb (129 hIgG1) creates a cancer-targeting mAb with significantly improved avidity and ensuing *in vitro* and *in vivo* antitumor activity

We recently described the generation of a sialyl-di-Lewis[a] recognizing mAb (129 mAb) with development potential for cancer immunotherapy (9). The 129 mAb has a more favorable tumor versus normal human tissue distribution compared with the above-described 88 mAb, resulting from wide-ranging tumor tissue binding, combined with very restricted normal tissue reactivity. Neither the hybridoma-produced FG129, a murine IgG1 mAb, nor the chimeric 129hIgG1, exhibited direct cytotoxicity. This led us to test the hypothesis that the introduction of the 23 above-selected mIgG3 constant region residues into the Fc region of 129hIgG1 would create an ""129G1 with direct cytotoxicity and improved avidity and thus exhibit superior clinical utility.

We evaluated the direct cytotoxicity of i129G1 on COLO205, previously shown to be a high-binding cancer cell line for FG129 (9). The i129G1 displayed significantly improved (compared with 129hIgG1) dose-dependent inhibition of proliferation (**Fig. 6A**; **Table 1**), with an EC_{50} of 45.6 nmol/L, as well as a significantly improved, but more modest, PI uptake (**Fig. 6B**). In comparison, negligible direct cytotoxicity was observed on the low to moderate binding ASPC1 or BXPC3 (Supplementary Fig. S4A and S4B), compared with the high-binding COLO205 (Supplementary Fig. S4C).

Published OnlineFirst June 12, 2020; DOI: 10.1158/0008-5472.CAN-19-3599

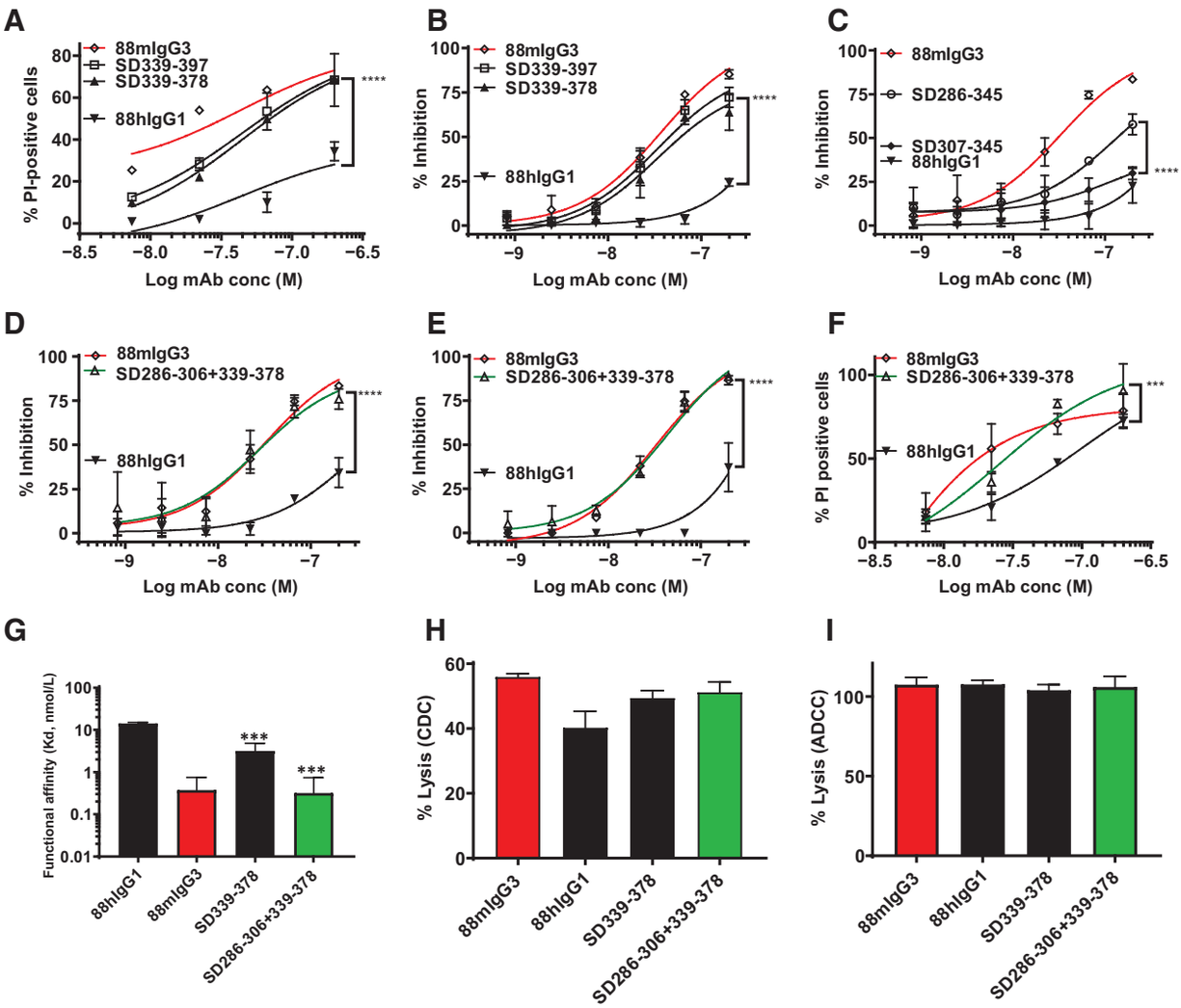

Figure 4.

Discontinuous regions consisting of 286–306 combined with 339–378 impart direct cytotoxicity and enhanced avidity, while maintaining immune effector functions. **A** and **B,** Significantly increased PI uptake (**A**) and proliferation inhibition (**B**) by SD339-378 compared with 88hIgG1 on HCT15. **C,** Significantly reduced proliferation inhibition by SD307-345 compared with SD286-345, suggesting a contribution by SD286-306. **D–F,** Significantly increased proliferation inhibition by the combination of SD286-306+339-378 compared with 88hIgG1 on HCT15 (**D**) and COLO205 (**E**), as well as PI uptake on COLO205 (**F**). **G,** Significantly increased avidity (SPR) by SD339-378 as well as SD286-306+339-378 compared with 88hIgG1. **H** and **I,** Maintenance of CDC activity on HCT15 (**H**) and ADCC on COLO205 (**I**) by SD339-378 as well as SD286-306+339-378 compared with 88hIgG1. Significance versus respective parental constructs was deduced from two-way ANOVA (direct cytotoxicity) or one-way ANOVA, with Dunnett's corrections for multiple comparisons (avidity, and effector functions). ***, $P \leq 0.001$; ****, $P \leq 0.0001$.

Next, we analyzed the avidity of i129G1 using a sialyl Lewis^a-APD-HSA–coated chip and SPR. The i129G1 mAb exhibited significantly improved avidity compared with 129hIgG1 (**Fig. 6C**; **Table 1**; Supplementary Fig. S3), resulting predominantly from an improvement in off-rate by almost two logs (2.6×10^{-4} s^{-1} and 5.5×10^{-6} s^{-1} for 129hIgG1 and i129G1, respectively). On COLO205, i129G1 maintained ADCC activity in the nanomolar range (EC_{50} 2.4 nmol/L), compared with 1.7 nmol/L for 129hIgG1, but the overall percentage lysis was significantly reduced (**Fig. 6D**; **Table 1**). The CDC activity of i129G1, however, was significantly increased compared with the parental 129hIgG1, with EC_{50} of 8.2 and 75 nmol/L, respectively (**Fig. 6E**; **Table 1**). The direct cytotoxicity as well as improved avidity of i129G1 led us to analyze its pore-forming ability on COLO205. The incubation of COLO205 with i129G1 caused the formation of large cell clumps with uneven surfaces, as well as the appearance of irregular pore-like structures (**Fig. 6F**). Incubation with 129hIgG1, at the same concentration, also led to a degree of cell clumping, but smaller and fewer clumps were observed, without evidence of pore formation.

The direct cytotoxicity and improved avidity of i129G1 directed us toward analyzing the *in vivo* antitumor activity of i129G1 in comparison with the parental 129hIgG1 in a COLO205 xenograft model. The i129G1 mAb instigated a significant reduction in tumor volume compared with vehicle control (two-way ANOVA, $P < 0.0001$, **Fig. 6G**; Supplementary Fig. S5), which remained significant when compared with 129hIgG1, thereby corroborating the *in vitro* results. No adverse effects on mean body weight were observed (**Fig. 6H**).

Published OnlineFirst June 12, 2020; DOI: 10.1158/0008-5472.CAN-19-3599

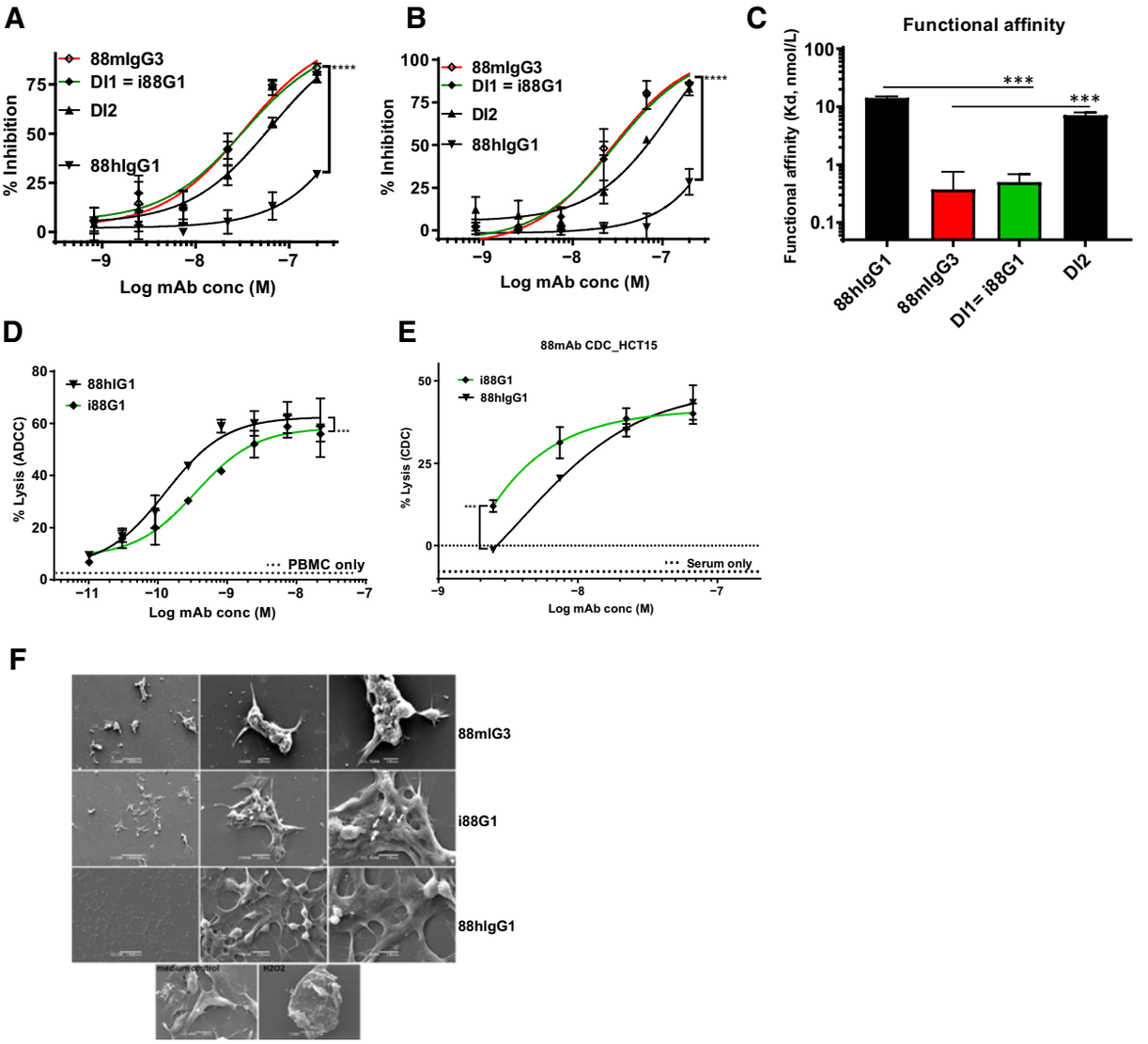

Figure 5.

i88G1 with direct cytotoxicity and enhanced avidity, while maintaining immune effector functions, exhibits pore forming ability. Reversion to human sequence of three residues in IEDB-predicted MHCII binding cluster 1 (Supplementary Fig. S2) created the lead candidate i88G1 (DI1). **A** and **B,** Significantly increased proliferation inhibition on HCT15 (**A**) and COLO205 (**B**) by i88G1 compared with 88hIgG1, now matching 88mIgG3 activity. Significance deduced from two-way ANOVA. DI2 displayed a consistent reduction in cytotoxicity compared with DI1. **C,** Significantly increased avidity (SPR) by i88G1 compared with 88hIgG1; significantly decreased avidity by DI2 compared with 88mIgG3. One-way ANOVA with Dunnett's corrections for multiple comparisons. **D** and **E,** Significantly reduced, yet remaining subnanomolar, ADCC (COLO205; **D**) as well as significantly improved CDC (HCT15; **E**) activity by i88G1 compared with 88hIgG1 (two-way ANOVA). **F,** Evidence of cellular detachment, aggregation, and pore formation (white arrows, irregular pores) by i88G1 on HCT15. ***, $P \leq 0.001$; ****, $P \leq 0.0001$.

In order to ascertain that our Fc-engineering approach had not affected the biopharmaceutical development potential of the i129G1 mAb, we evaluated its *in vitro* FcRn binding ability, as well as its solution aggregation status using a range of biophysical and biochemical approaches. *In vitro* binding of i129G1 to rhFcRn at pH 6.0 and pH 7.0 was compared with the parental 129hIgG1 as well as clinically validated ipilimumab, also a hIgG1. At pH 6.0, 129hIgG1 as well as i129G1 display improved binding compared with ipilimumab. Furthermore, i129G1 exhibited significantly improved rhFcRn binding compared with 129hIgG1 at the highest concentrations tested (**Fig. 6I**). Some rhFcRn binding was observed at pH 7.0, mainly at the higher concentrations, with the parental 129hIgG1 displaying higher reactivity compared with i129G1. Next, we evaluated the solution-phase characteristics of i129G1 compared with the parental 129hIgG1 using SEC-MALS and AUC. The SEC-MALS profile of 129hIgG1 as well as i129G1 were similar, containing a main peak (16–18 mL) consistent with an antibody monomer as well as two minor peaks corresponding to higher molecular weight (MW) species [15 and 8 mL (void volume), respectively; **Fig. 6J, i**]. AUC profiles of both mAbs across the three concentrations tested revealed a slight increase in the number of higher MW species for i129v1, the main mAb monomer peak being 80.6% ± 2.6% and 67.6% ± 2.3% of all

Published OnlineFirst June 12, 2020; DOI: 10.1158/0008-5472.CAN-19-3599

Table 1. Overview of the functional characteristics of the improved constructs.

	Biological activity characteristics				
mAb	Avidity[a] Kd (nmol/L)	Direct cytotoxicity[b] EC_{50} (nmol/L)	ADCC EC_{50} (nmol/L)	CDC EC_{50} (nmol/L)	Pore-forming ability
88mIgG3	0.3	26.7	ND	ND	+++
88hIgG1	48.3	N/A	0.13	3.9	–
i88G1	0.5	29.4	0.35	0.1	++
129hIgG1	2.5	N/A	1.7	75.3	–
i129G1	0.005	45.6	2.4	8.2	++

Abbreviations: N/A, not appropriate; ND, not determined.
[a]Sensorgrams underlying the avidity determination are shown in Supplementary Fig. S3.
[b]Deduced from proliferation inhibition on COLO205.

species detected in the sample for 129hIgG1 and i129v1, respectively (**Fig. 6J, ii**). The latter analysis prompted us to investigate whether the small increase in higher molecular weight species in the i129v1 sample would lead to complement activation in normal human serum in the absence of antigen engagement. A commercial C4d detection kit (indicating classical complement pathway activation) was used, and the analysis was performed with serum from three healthy donors. Whereas HA mAb instigated a significant increase in C4d levels upon incubation with human serum, neither i129G1, nor 129hIgG1, caused significant elevation of C4d above the background (**Fig. 6J, iii**).

Discussion

Whereas unmodified cancer glycan–targeting mAbs often exhibit antitumor activity in preclinical animal models, they perform disappointingly in the clinic (3, 22–24). One possible explanation is that mIgG3 anti-glycan mAbs exhibited direct cytotoxic activity, which was significantly reduced when chimerized or humanized to hIgG1 (10–13). Similarly, the Lewis$^{a/c/x}$ FG88.2 used in this study, a mIgG3 isotype, exhibited high avidity as well as direct cytotoxicity upon binding to high target-expressing cancer cells (7), both of which were significantly reduced on chimerization to hIgG1.

It is perhaps not surprising that the direct cytotoxicity of cancer glycan–targeting mIgG3 mAbs was reduced upon chimerization to a hIgG1 isotype, in view of the well-documented effect of mAb constant regions on variable region affinity and specificity (25–30). However, constant region-driven allosteric effects (intramolecular) tend to be mAb and target specific (27). Greenspan and colleagues on the other hand surmised that mIgG3 intermolecular cooperativity—enhanced binding through stabilization of noncovalent interactions between neighboring bound mAbs—brought about increased avidity for multivalent antigen and ensuing isotype restriction (18, 31, 32). Improved avidity, resulting mainly from slower kinetic off-rates by mIgG3 mAbs, compared with other isotypes, has also been observed by others and resulted in more effective binding at high epitope density (33–37). A number of multimerization strategies with human isotype mAbs have attempted to recreate this increased avidity for cancer antigens, but these were inefficient or unstable (38–40). In addition, a plethora of Fc-engineering strategies, mostly to affect mAb effector functions (ADCC and CDC), through modifying FcγR or C1q binding, as well as mAb half-live, via FcRn engagement, have been described (41, 42). Interestingly, crystal packing-induced mAb oligomerization through Fc:Fc interactions in a number of human mAb isotypes (43–46) formed the basis of a recently described hexameric mAb platform for improved complement activation (47–49). The aforementioned HexaBody technology centered on two positions (E345 and E430) the mutation of which significantly enhanced CDC activity, without affecting other key pharmacokinetic and biopharmaceutical properties. Our approach, on the other hand, focused on improving direct cell killing of glycan-targeting mAbs through engineering increased avidity, mirroring a common ability observed for the murine IgG3 isotype. Advantageously, there is no requirement for complement or immune effector cells and as such our strategy may be less susceptible to immunesuppression in the tumor microenvironment.

In the current study, we describe the creation of hIgG1 anti-glycan mAbs with increased avidity and direct cytotoxic activity through the transfer of selected mIgG3 constant region residues. Candidate residues were identified through screens based on increased direct cytotoxicity and avidity, when introduced into hIgG1 (gain-of-function), and/or decreased direct cytotoxicity and avidity when replaced by the respective hIgG1 residues in mIgG3 (loss-of-function), using the Lewis$^{a/c/x}$ FG88.2.

Differences in segmental flexibility between the two mAbs due to the changed CH1 and hinge regions as well as a direct contribution by murine IgG3 CH1 were ruled out, as the introduction of murine IgG3 CH1 into 88hIgG1 did not increase direct cytotoxicity. Neither did the introduction of hIgG1 CH1 into 88mIgG3 decrease direct cytotoxicity. The murine IgG3 hinge region has somewhat greater flexibility, compared with other murine isotypes (50), but an involvement of the hinge region, in isolation, is unlikely to be solely responsible for the observed direct cytotoxicity and improved avidity, as was recently shown for an erythrocyte glycan-binding mIgG3 mAb (36).

Focusing on the mIgG3 Fc region, a major contribution by CH3 was identified, with effects evident in improved cytotoxicity as well as avidity, the latter mainly the result of a decreased dissociation rate. A minor contribution by CH2 was only evident when screened via the loss-of-function approach, suggesting a less dominant effect. Similarly, in this setting, the decreased avidity coincided with an increased dissociation rate. An analogous analysis identified a contribution by both CH2 and CH3 domains in protective mIgG3 mAbs directed at the capsular antigen of *Bacillus anthracis* (37). More recently, Klaus and colleagues performed a comprehensive evaluation of mIgG3 constant region contributions to blood glycan avidity (36). Although they attributed a stronger role for the mIgG3 CH2 domain, an effect of CH3 domain was also noted and led to the overall conclusion that the increased avidity of the mIgG3 isotype was likely the result of additive effects through CH domain interplay.

Further dissection of the combined CH2CH3 region through subdomain analysis revealed full regain of 88mIgG3 direct cytotoxicity by a section, encompassing the CH2CH3 junction ("elbow"), residues

Published OnlineFirst June 12, 2020; DOI: 10.1158/0008-5472.CAN-19-3599

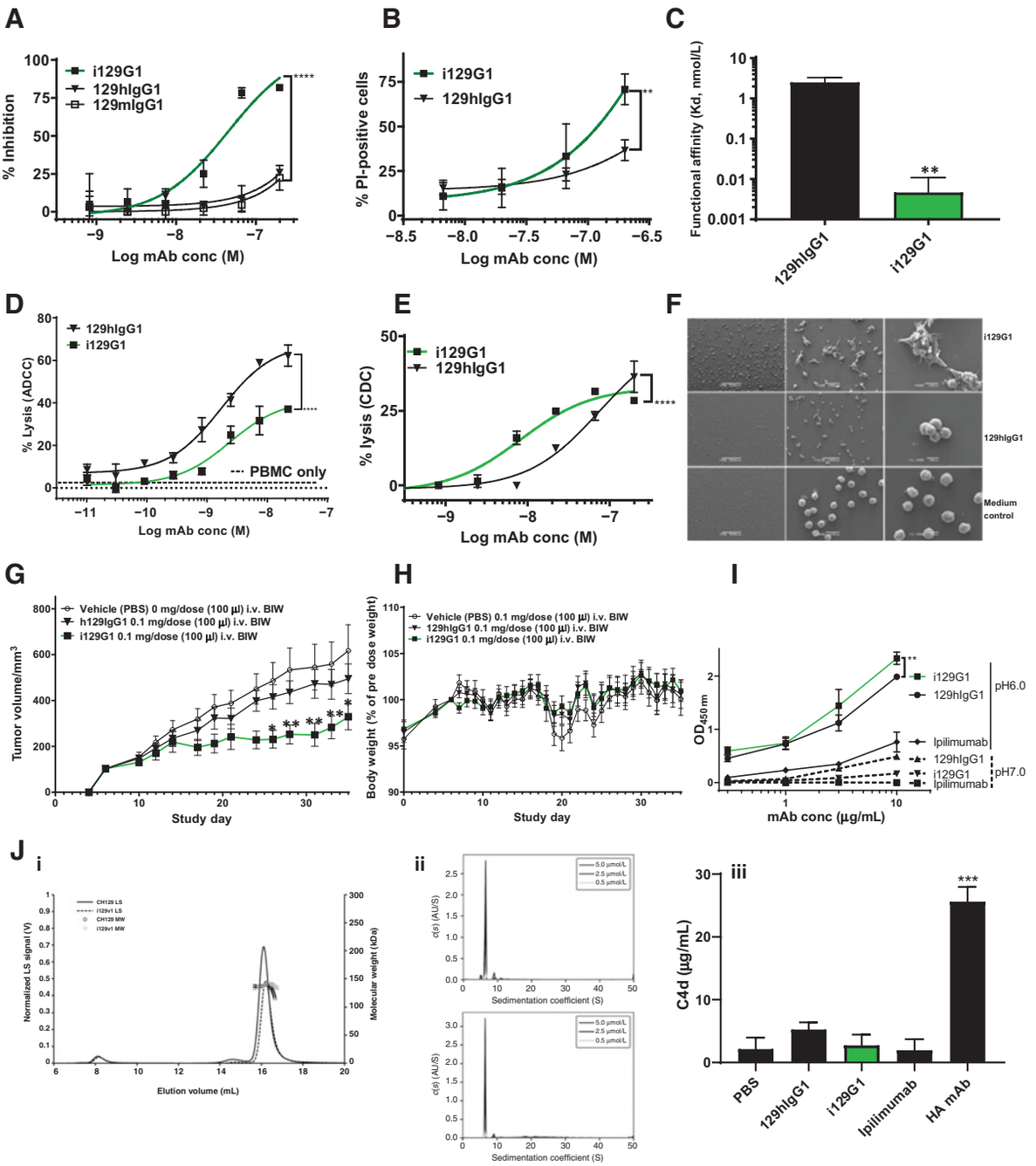

Figure 6.

i129G1, derived from a noncytotoxic mIgG1 mAb, exhibits significant direct cytotoxicity, enhanced avidity, pore-forming ability, as well as significant *in vivo* tumor control. **A** and **B,** Significantly increased proliferation inhibition (**A**) and PI uptake (**B**) on COLO205 by i129G1 compared with 129hIgG1. Direct cell killing of low to moderate binding cancer cell lines was negligible (Supplementary Fig. S4). **C,** Significantly increased functional affinity (SPR) by i129G1 compared with 129hIgG1. **D,** i129G1 maintains nanomolar ADCC activity on COLO205, but with significantly reduced overall lysis compared with h129hIgG1. **E,** Nanomolar CDC activity by i129G1 on COLO205 is significantly increased compared with 129hIgG1. **F,** Evidence of cellular detachment, aggregation, and pore-forming ability by i129G1 on COLO205 using SEM. White arrows, irregular pores. **G,** Significant *in vivo* tumor control by i129G1 compared with vehicle control and compared with 129hIgG1 in a COLO205 xenograft model (Balb/c nude mice). Individual tumor growth curves are shown in Supplementary Fig. S5. **H,** No significant effect on mean body weight during the course of the mouse study. **I,** Dose-dependent binding of rhFcRn by i129G1 and 129hIgG1 at pH6.0. Significantly increased binding by i129G1 compared with 129hIgG1 at the top two concentrations. Negligible binding at pH 7.0 by both constructs. **J, i,** Similar SEC-MALS profiles for i129G1 compared with 129hIgG1. **J, ii,** A small increase in higher MW species is evident in i129G1 (bottom) compared with 129hIgG1 (top) via AUC. **J, iii,** No significant increase in C4d generation upon incubation with human serum by i129G1, compared with 129hIgG1. Significance versus respective parental constructs was deduced from two-way ANOVA (direct cytotoxicity, effector functions, rhFcRn binding, *in vivo* tumor control) or one-way ANOVA (functional affinity and C4d detection), with Dunnett's corrections for multiple comparisons. *, $P \le 0.05$; **, $P \le 0.01$; ***, $P \le 0.001$; ****, $P \le 0.0001$.

Published OnlineFirst June 12, 2020; DOI: 10.1158/0008-5472.CAN-19-3599

286–397. This stretch of residues contained the combined effects of the dominant CH3 element (residues 339–397) as well as the subdominant CH2 contribution (residues 286–345). Although the CH3 element (339–397) in isolation led to an improved avidity, as well as cytotoxicity, unfortunately, it coincided with significantly reduced CDC compared with 88hIgG1. This is likely an indirect, conformational, effect on C1q binding, as, although close to known C1q interacting residues, none of the 339–397 residues are directly interacting (47, 51). It however necessitated the analysis of residues in the region of 286–397 for further refinement of contributing elements.

The introduction into 88hIgG1 of a discontinuous section comprising residues 286–306 and 339–378 recapitulated 88mIgG3 cytotoxicity and avidity, while maintaining immune effector functions (ADCC and CDC). The likely explanation for the greater than anticipated number of mIgG3 residues required for increased avidity through intermolecular cooperativity is the combined effect of directly interacting as well as conformational residues, the latter potentially creating a permissive framework. A role for charge distribution patterns, notably in CH2, can also not be ruled out, as it has been shown to enhance mIgG3 binding to negatively charged multivalent antigen and is distinct from hIgG1 (36, 37).

The introduction of 26 mIgG3 in hIgG1 may create MHCII-binding epitopes that have the potential to drive HAMA responses in patients. IEDB analysis of the 26 mIgG3 residue-containing hybrid 88hIgG1 revealed two clusters (residues 294–315 and 365–378), one containing several potentially high-scoring epitopes. Residues in cluster 1, at positions 294, 300, and 305, were reverted to human sequence with maintained avidity and direct cytotoxicity. On the other hand, reverting residues at positions 351 and 371 (cluster 2, with weaker binding scores) led to a small but significant decreased cytotoxicity, hence were maintained in the final construct. Importantly, this superior 88hIgG1 hybrid mAb, with mIgG3-matching direct cytotoxicity and avidity, induced cellular aggregation, pore formation, and cell lysis on high-binding HCT15, suggesting a similar cell killing mechanism compared with the parental FG88.2 (7). The pore formation and eventual cell lysis share similar cellular disintegration features with necroptosis, but cannot be distinguished from necrosis or secondary necrosis (52). The eventual outcome from the released DAMPs—constitutive or induced as a result of activated stress pathways—during this inflammatory cell death depends on the cellular environment as well as the underlying signaling cascades, but collectively has the potential to create an inflammatory environment that may further enhance immune effector functions and/or instigate an adaptive immune response through cross-presentation of released tumor antigens (16, 53). Advantageously, i88G1 maintained immune effector functions with CDC activity being significantly improved, and ADCC activity being somewhat reduced, compared with 88hIgG1. As the Fc residues involved in FcgammaRIIa/RIIIa binding are predominantly located in the lower hinge and adjacent top of CH2 region, it is unlikely that our introduced changes have a direct effect on this interaction, but we cannot rule out an indirect effect (54).

Further validation of our approach came from the introduction of the selected 23 mIgG3 residues into the sialyl-di-Lewis[a] targeting 129hIgG1, that has a more favorable normal tissue distribution while targeting a wide range of tumor tissues on tumor microarray analyses, notably binding over 70% of pancreatic, and over 30% of gastric and colorectal tumor tissues, as well as over 20% of ovarian and non–small cell lung cancer tumor tissues (9). Interestingly, the hybridoma-produced parental FG129 is a mIgG1 that lacks direct cytotoxic ability. Thus, the creation of i129G1 with significantly improved avidity, through a slower dissociation rate, compared with 129hIgG1, coinciding with nanomolar direct cell killing ability on COLO205, suggests that our approach may have broader applicability, as well as being relevant for immunomodulatory mAbs that rely on avidity effects (41). The direct cell killing exerted by i129G1 manifested itself in a similar manner as for i88G1: mAb-induced cellular aggregation followed by pore formation and eventual cell lysis. The introduction of the mIgG3 residues into i129G1 mAb had a mixed effect on effector functions: while overall ADCC-induced cell lysis was significantly reduced, i129G1 maintained nanomolar EC_{50}. The CDC activity of i129G1 on the other hand was significantly increased. This mirrored the results obtained with i88G1, albeit with a stronger reduction in ADCC for i129G1, suggesting that the nature of the glycotarget also affects ADCC potency: whereas the FG88.2 targets glycoproteins as well as glycolipids, the FG129 only targets glycoproteins. Our improved mAb construct, i129G1, exhibited significant tumor volume reduction in a COLO205 xenograft model in nude mice. Remarkably, i129G1 displayed effective tumor control that was significantly better than 129hIgG1, the latter exhibiting no significant tumor reduction, further emphasizing the value of direct cytotoxic ability.

In addition, it was important to ascertain that our Fc engineering had not affected the solution self-association of i129G1. Although the biophysical analysis suggested a small increase in the proportion of higher MW species in the i129G1 sample, more apparent from AUC than SEC-MALS, this did not result in a significantly increased C4d generation upon incubation with healthy human donor serum. We did not observe a reduction in rhFcRn by i129G1 binding, suggesting that the pharmacokinetic aspects equally had not been compromised by our Fc engineering.

The creation of improved cancer glycan–targeting mAbs, with enhanced avidity as well as direct cytotoxicity, through establishing intermolecular cooperativity binding, may lead to superior clinical utility. In addition, it is plausible that mAb multimerization upon glycan target engagement through alternative strategies may equally lead to increased avidity and ensuing direct cytotoxicity. Our approach may also have value for mAbs targeting cancer-associated proteins, where longer target residence time may lead to more profound biological effects, but this remains to be validated. Importantly, reinstating the unusual, proinflammatory cell killing mode observed for many glycan-targeting mIgG3 mAbs, into the hIgG1 framework, opens the door to combination immunotherapy.

Disclosure of Potential Conflicts of Interest

M. Vankemmelbeke reports grants from MRC-UK during the conduct of the study and other funding from Scancell Ltd. (salary) outside the submitted work as well as a patent for P125250GB (pending). R.S. McIntosh reports grants from MRC DPFS during the conduct of the study as well as a patent for P125250GB (pending). T. Kirk reports grants from MRC during the conduct of the study and personal fees from Scancell Limited (salary) outside the submitted work. I. Daniels reports other funding from Scancell Ltd. (salary) during the conduct of the study and other funding from Scancell Ltd. (salary) outside the submitted work. M. Patsalidou reports grants from MRC-UK during the conduct of the study. J.M. Ramage reports grants from MRC during the conduct of the study. I. Spendlove reports grants from MRC during the conduct of the study. L.G. Durrant reports other funding from Scancell Ltd. (I am a director and shareholder of Scancell Ltd.) during the conduct of the study as well as a patent for P125250GB (pending). No potential conflicts of interest were disclosed by the other authors.

Authors' Contributions

M. Vankemmelbeke: Conceptualization, formal analysis, funding acquisition, investigation, methodology, writing-original draft, writing-review and editing. **R.S. McIntosh:** Conceptualization, formal analysis, funding acquisition, investigation, methodology, writing-review and editing. **J.X. Chua:** Resources, methodology. **T. Kirk:** Formal analysis, investigation, methodology. **I. Daniels:** Formal analysis, investigation. **M. Patsalidou:** Investigation, methodology. **R. Moss:** Resources. **T. Parsons:** Project administration, writing-review and

editing. **D. Scott:** Resources, methodology. **G. Harris:** Formal analysis, investigation, methodology. **J.M. Ramage:** Conceptualization, funding acquisition, writing-review and editing. **I. Spendlove:** Conceptualization, funding acquisition. **L.G. Durrant:** Conceptualization, supervision, funding acquisition, validation, writing-review and editing.

Acknowledgments

This work was supported by MRC-DPFS funding (MR/M015564/1) and Scancell Ltd.

We are grateful for expert technical assistance with EM work (Denise Mclean, Advanced Microscopy Unit, School of Life Sciences) and for Biacore access (Prof. Stephanie Allen, School of Pharmacy), University of Nottingham. This work was supported by a Developmental Pathway Funding Scheme grant from MRC-UK (MR/M015564/1).

The costs of publication of this article were defrayed in part by the payment of page charges. This article must therefore be hereby marked *advertisement* in accordance with 18 U.S.C. Section 1734 solely to indicate this fact.

Received November 21, 2019; revised March 25, 2020; accepted June 5, 2020; published first June 12, 2020.

References

1. Dalziel M, Crispin M, Scanlan CN, Zitzmann N, Dwek RA. Emerging principles for the therapeutic exploitation of glycosylation. Science 2014;343:1235681.
2. RodrIguez E, Schetters STT, van Kooyk Y. The tumour glyco-code as a novel immune checkpoint for immunotherapy. Nat Rev Immunol 2018;18:204–11.
3. Burris HA 3rd, Rosen LS, Rocha-Lima CM, Marshall J, Jones S, Cohen RB, et al. Phase 1 experience with an anti-glycotope monoclonal antibody, RAV12, in recurrent adenocarcinoma. Clin Cancer Res 2010;16:1673–81.
4. Labrada M, Dorvignit D, Hevia G, Rodriguez-Zhurbenko N, Hernandez AM, Vazquez AM, et al. GM3(Neu5Gc) ganglioside: an evolution fixed neoantigen for cancer immunotherapy. Semin Oncol 2018;45:41–51.
5. Hege KM, Bergsland EK, Fisher GA, Nemunaitis JJ, Warren RS, McArthur JG, et al. Safety, tumor trafficking and immunogenicity of chimeric antigen receptor (CAR)-T cells specific for TAG-72 in colorectal cancer. J Immunother Cancer 2017;5:22.
6. Ladenstein R, Potschger U, Valteau-Couanet D, Luksch R, Castel V, Yaniv I, et al. Interleukin 2 with anti-GD2 antibody ch14.18/CHO (dinutuximab beta) in patients with high-risk neuroblastoma (HR-NBL1/SIOPEN): a multicentre, randomised, phase 3 trial. Lancet Oncol 2018;19:1617–29.
7. Chua JX, Vankemmelbeke M, McIntosh RS, Clarke PA, Moss R, Parsons T, et al. Monoclonal antibodies targeting LecLex-related glycans with potent antitumor activity. Clin Cancer Res 2015;21:2963–74.
8. Noble P, Spendlove I, Harding S, Parsons T, Durrant LG. Therapeutic targeting of Lewis(y) and Lewis(b) with a novel monoclonal antibody 692/29. PLoS One 2013;8:e54892.
9. Tivadar ST, McIntosh RS, Chua JX, Moss R, Parsons T, Zaitoun AM, et al. Monoclonal antibody targeting Sialyl-di-Lewis(a)-containing internalizing and noninternalizing glycoproteins with cancer immunotherapy development potential. Mol Cancer Ther 2020;19:790–801.
10. Loo D, Pryer N, Young P, Liang T, Coberly S, King KL, et al. The glycotope-specific RAV12 monoclonal antibody induces oncosis in vitro and has antitumor activity against gastrointestinal adenocarcinoma tumor xenografts in vivo. Mol Cancer Ther 2007;6:856–65.
11. Faraj S, Bahri M, Fougeray S, El Roz A, Fleurence J, Veziers J, et al. Neuroblastoma chemotherapy can be augmented by immunotargeting O-acetyl-GD2 tumor-associated ganglioside. Oncoimmunology 2017;7:e1373232.
12. Roque-Navarro L, Chakrabandhu K, de Leon J, Rodriguez S, Toledo C, Carr A, et al. Anti-ganglioside antibody-induced tumor cell death by loss of membrane integrity. Mol Cancer Ther 2008;7:2033–41.
13. Welt S, Carswell EA, Vogel CW, Oettgen HF, Old LJ. Immune and nonimmune effector functions of IgG3 mouse monoclonal antibody R24 detecting the disialoganglioside GD3 on the surface of melanoma cells. Clin Immunol Immunopathol 1987;45:214–29.
14. Zheng JY, Tan HL, Matsudaira PT, Choo A. Excess reactive oxygen species production mediates monoclonal antibody-induced human embryonic stem cell death via oncosis. Cell Death Differ 2017;24:546–58.
15. Hernandez AM, Rodriguez N, Gonzalez JE, Reyes E, Rondon T, Grinan T, et al. Anti-NeuGcGM3 antibodies, actively elicited by idiotypic vaccination in non-small cell lung cancer patients, induce tumor cell death by an oncosis-like mechanism. J Immunol 2011;186:3735–44.
16. Galluzzi L, Buque A, Kepp O, Zitvogel L, Kroemer G. Immunogenic cell death in cancer and infectious disease. Nat Rev Immunol 2017;17:97–111.
17. Cooper LJ, Schimenti JC, Glass DD, Greenspan NS. H chain C domains influence the strength of binding of IgG for streptococcal group A carbohydrate. J Immunol 1991;146:2659–63.
18. Greenspan NS, Dacek DA, Cooper LJ. Cooperative binding of two antibodies to independent antigens by an Fc-dependent mechanism. FASEB J 1989;3:2203–7.
19. Yoo EM, Wims LA, Chan LA, Morrison SL. Human IgG2 can form covalent dimers. J Immunol 2003;170:3134–8.
20. Metheringham RL, Pudney VA, Gunn B, Towey M, Spendlove I, Durrant LG. Antibodies designed as effective cancer vaccines. MAbs 2009;1:71–85.
21. Jawa V, Cousens LP, Awwad M, Wakshull E, Kropshofer H, De Groot AS. T-cell dependent immunogenicity of protein therapeutics: preclinical assessment and mitigation. Clin Immunol 2013;149:534–55.
22. Mita MM, Nemunaitis J, Grilley-Olson J, El-Rayes B, Bekaii-Saab T, Harvey RD, et al. Phase 1 study of CEP-37250/KHK2804, a tumor-specific anti-glycoconjugate monoclonal antibody, in patients with advanced solid tumors. Target Oncol 2016;11:807–14.
23. Horta ZP, Goldberg JL, Sondel PM. Anti-GD2 mAbs and next-generation mAb-based agents for cancer therapy. Immunotherapy 2016;8:1097–117.
24. Forero A, Shah J, Carlisle R, Triozzi PL, LoBuglio AF, Wang WQ, et al. A phase I study of an anti-GD3 monoclonal antibody, KW-2871, in patients with metastatic melanoma. Cancer Biother Radiopharm 2006;21:561–8.
25. Janda A, Bowen A, Greenspan NS, Casadevall A. Ig constant region effects on variable region structure and function. Front Microbiol 2016;7:22.
26. Casadevall A, Janda A. Immunoglobulin isotype influences affinity and specificity. Proc Natl Acad Sci U S A 2012;109:12272–3.
27. Yang D, Kroe-Barrett R, Singh S, Roberts CJ, Laue TM. IgG cooperativity - Is there allostery? Implications for antibody functions and therapeutic antibody development. MAbs 2017;9:1231–52.
28. Cooper LJ, Shikhman AR, Glass DD, Kangisser D, Cunningham MW, Greenspan NS. Role of heavy chain constant domains in antibody-antigen interaction. Apparent specificity differences among streptococcal IgG antibodies expressing identical variable domains. J Immunol 1993;150:2231–42.
29. Torres M, Casadevall A. The immunoglobulin constant region contributes to affinity and specificity. Trends Immunol 2008;29:91–7.
30. McCloskey N, Turner MW, Steffner P, Owens R, Goldblatt D. Human constant regions influence the antibody binding characteristics of mouse-human chimeric IgG subclasses. Immunology 1996;88:169–73.
31. Greenspan NS, Cooper LJ. Cooperative binding by mouse IgG3 antibodies: implications for functional affinity, effector function, and isotype restriction. Springer Semin Immunopathol 1993;15:275–91.
32. Greenspan NS, Cooper LJ. Intermolecular cooperativity: a clue to why mice have IgG3? Immunol Today 1992;13:164–8.
33. Cooper LJ, Robertson D, Granzow R, Greenspan NS. Variable domain-identical antibodies exhibit IgG subclass-related differences in affinity and kinetic constants as determined by surface plasmon resonance. Mol Immunol 1994;31:577–84.
34. Yelton D. An IgG3 antitumor antibody showing cooperative binding mediated by the constant region. Abstract, BIAsymposium 1992 Meeting Review. Pharmacia Biosensor 1992.
35. Loibner H, Janzek E, Plot R. Fc-dependent binding self-cooperativity of a murine IgG3 antitumor mAb as demonstrated by biospecific interaction analysis - comparison with murine switch variants and mouse/human chimeras. Abstract, Second European BIAsymposium 1992. Pharmacia Biosensor 1992.
36. Klaus T, Bereta J. CH2 domain of mouse IgG3 governs antibody oligomerization, increases functional affinity to multivalent antigens and enhances hemagglutination. Front Immunol 2018;9:1096.
37. Hovenden M, Hubbard MA, Aucoin DP, Thorkildson P, Reed DE, Welch WH, et al. IgG subclass and heavy chain domains contribute to binding and protection by mAbs to the poly gamma-D-glutamic acid capsular antigen of Bacillus anthracis. PLoS Pathog 2013;9:e1003306.

38. Wolff EA, Schreiber GJ, Cosand WL, Raff HV. Monoclonal antibody homodimers: enhanced antitumor activity in nude mice. Cancer Res 1993; 53:2560–5.
39. Hu J, Liu X, Hughes D, Esteva FJ, Liu B, Chandra J, et al. Herceptin conjugates linked by EDC boost direct tumor cell death via programmed tumor cell necrosis. PLoS One 2011;6:e23270.
40. Caron PC, Laird W, Co MS, Avdalovic NM, Queen C, Scheinberg DA. Engineered humanized dimeric forms of IgG are more effective antibodies. J Exp Med 1992;176:1191–5.
41. Wang X, Mathieu M, Brezski RJ. IgG Fc engineering to modulate antibody effector functions. Protein Cell 2018;9:63–73.
42. Carter PJ. Potent antibody therapeutics by design. Nat Rev Immunol 2006; 6:343–57.
43. Saphire EO, Parren PW, Pantophlet R, Zwick MB, Morris GM, Rudd PM, et al. Crystal structure of a neutralizing human IGG against HIV-1: a template for vaccine design. Science 2001;293:1155–9.
44. Davies AM, Rispens T, Ooijevaar-de Heer P, Gould HJ, Jefferis R, Aalberse RC, et al. Structural determinants of unique properties of human IgG4-Fc. J Mol Biol 2014;426:630–44.
45. Davies AM, Jefferis R, Sutton BJ. Crystal structure of deglycosylated human IgG4-Fc. Mol Immunol 2014;62:46–53.
46. Wu Y, West AP Jr, Kim HJ, Thornton ME, Ward AB, Bjorkman PJ. Structural basis for enhanced HIV-1 neutralization by a dimeric immunoglobulin G form of the glycan-recognizing antibody 2G12. Cell Rep 2013;5:1443–55.
47. Ugurlar D, Howes SC, de Kreuk BJ, Koning RI, de Jong RN, Beurskens FJ, et al. Structures of C1-IgG1 provide insights into how danger pattern recognition activates complement. Science 2018;359:794–7.
48. de Jong RN, Beurskens FJ, Verploegen S, Strumane K, van Kampen MD, Voorhorst M, et al. A novel platform for the potentiation of therapeutic antibodies based on antigen-dependent formation of IgG hexamers at the cell surface. PLoS Biol 2016;14:e1002344.
49. Diebolder CA, Beurskens FJ, de Jong RN, Koning RI, Strumane K, Lindorfer MA, et al. Complement is activated by IgG hexamers assembled at the cell surface. Science 2014;343:1260–3.
50. Dangl JL, Wensel TG, Morrison SL, Stryer L, Herzenberg LA, Oi VT. Segmental flexibility and complement fixation of genetically engineered chimeric human, rabbit and mouse antibodies. EMBO J 1988;7:1989–94.
51. Duncan AR, Winter G. The binding site for C1q on IgG. Nature 1988;332: 738–40.
52. Vanden Berghe T, Vanlangenakker N, Parthoens E, Deckers W, Devos M, Festjens N, et al. Necroptosis, necrosis and secondary necrosis converge on similar cellular disintegration features. Cell Death Differ 2010;17:922–30.
53. Yatim N, Cullen S, Albert ML. Dying cells actively regulate adaptive immune responses. Nat Rev Immunol 2017;17:262–75.
54. Wines BD, Powell MS, Parren PW, Barnes N, Hogarth PM. The IgG Fc contains distinct Fc receptor (FcR) binding sites: the leukocyte receptors Fc gamma RI and Fc gamma RIIa bind to a region in the Fc distinct from that recognized by neonatal FcR and protein A. J Immunol 2000;164:5313–8.

Published OnlineFirst June 12, 2020; DOI: 10.1158/0008-5472.CAN-19-3599

Cancer Research
The Journal of Cancer Research (1916–1930) | The American Journal of Cancer (1931–1940)

AACR American Association for Cancer Research

Engineering the Human Fc Region Enables Direct Cell Killing by Cancer Glycan–Targeting Antibodies without the Need for Immune Effector Cells or Complement

Mireille Vankemmelbeke, Richard S. McIntosh, Jia Xin Chua, et al.

Cancer Res 2020;80:3399-3412. Published OnlineFirst June 12, 2020.